



Numerical Investigation of the Time-of-Flight and Wave Energy Dependent Hybrid Method for Structural Damage Detection

Alaa Diab¹ · Tamara Nestorović¹

Received: 31 December 2022 / Revised: 6 May 2023 / Accepted: 21 May 2023 / Published online: 14 June 2023
© The Author(s) 2023

Abstract

Background Structural damage can be caused by various factors such as aging, environmental conditions, and unexpected events like earthquakes. Early detection of damage is crucial to prevent further deterioration, avoid catastrophic failure, and reduce maintenance costs. Damage detection methods that use piezoelectric sensors have gained popularity due to their non-destructive and non-invasive nature. Despite the progress made in the field of damage detection using piezoelectric sensors, there is still a need to improve the accuracy and reliability of those methods.

Objective This study aims to contribute to this by investigating the damage detection hybrid method, which uses the time-of-flight (ToF) criteria of acquired signals besides the energy loss damage index (DI) between damaged and intact states of a specimen, and exploring its possible improvements. The improvement potential in the investigated method regarding the signal processing details and the specification of the ToF used within the method, where the lack of information has been identified. Thus, the present study concentrates on those factors to get more benefit of the suggested method and extend its applicability.

Results The investigated factors play significant role in the accuracy and reliability of the method. By analyzing these criteria, this study contributes to the development of more advanced and reliable damage detection methods that can be applied to a wide range of structures, improving the ability to assess their structural health and safety. This study provides a better understanding of the hybrid method and contributes to the development of more accurate and reliable damage detection methods. The results of this study indicate that the proposed hybrid method effectively detects damage in the structural components under investigation with high accuracy and reliability.

Methods A 2D concrete plate is utilized to apply the proposed methodology. Hereby, various ToF criteria, truncation strategies of the signals, and the number of piezoelectric transducers used in the numerical experiment are examined to investigate their impact on the damage detection accuracy.

Conclusion Performance of the method was found to be significantly affected by selection of the investigated parameters, as well as of the number and placement of sensors. The findings suggest that a thorough analysis of these criteria can lead to further improvements in the accuracy and reliability of damage detection methods.

Keywords Damage index (DI) · Time-of-flight (ToF) · Damage localization · Signal processing

List of Symbols

Variables

α	Alfa proportionality constant for the mass damping (–)
β	Beta proportionality constant for the stiffness damping (–)
ξ	Damping ratio (–)
ω	Angular frequency of the system [1/sec]
k_{ω}	Absorption attenuation coefficient of the mechanical elastic wave (–)
A_1	Peak amplitude at the first sensor [m]
A_2	Peak amplitude at the second sensor [m]

✉ Alaa Diab
alaa.diab@rub.de
Tamara Nestorović
tamara.nestorovic@rub.de

¹ Mechanics of Adaptive Systems, Ruhr-Universität Bochum, Bochum, Germany

C	Damping matrix [Ns/m]
C_L	Longitudinal wave propagation velocity [m/s]
E	Young's modulus of the material [Pa]
$E_{(,),k}$	The energy of each decomposed signal [m^2]
E_d	The energy of the specimen in the damaged state [m^2]
E_h	The energy of the specimen in the intact state [m^2]
f	Frequency of the propagated wave [Hz]
K	Stiffness matrix [N/m]
l_1	Distance of a sensor at reference position from the actuator [m]
l_2	Distance of a second sensor at reference position from the actuator [m]
Δl	The wave propagation distance between two sensors [m]
M	Mass matrix [kg]
n	Number of cycles of vibration [cycle]
$P_{(t)}$	The excitation by the actuator [V]
t_{int}	Time interval of a signal to travel between two Actuators/Sensors [sec]
T	Wave period of excitation signal [sec]
t_1	Time for the wave to travel from an actuator to a sensor at distance l_1 [sec]
t_2	Time for the wave to travel from an actuator to a sensor at distance l_2 [sec]
u	Vibration amplitude between one cycle [m]
u_n	Vibration amplitude between n cycle [m]
X_S	Vector of the decomposed signals (–)
X_j	Vector of the j-th decomposed signal with a total of m sampling data (–)

Abbreviations

AS-path	The formed line between the Actuator and a Sensor within the specimen
BB	Building block
DI	Damage index
ED	Euclidean Distance ([m])
ECD	Energy curvature difference
NDM	Non-destructive methods
PZTs	Piezoelectric transducers
RMSD	Root mean square deviation
SHM	Structural Health Monitoring
SMI	Structural mechanical impedance
ToF	The time of flight for the signal to reach a sensor ([sec])
ToFi	Time of flight for the signal to reach a sensor in the intact state [sec]
ToFd	Time of flight for the signal to reach a sensor in the damaged state [sec]
ToF1	The time of flight determined based on the first zero crossing [sec]

ToF2	The time of flight determined based on the threshold of the max amplitude of the signal [sec]
ToF3	The time of flight determined based on the P-Phase method [sec]
UASs	Unmanned aerial systems (–)
WD	Excitation wave duration that includes the whole wave ([sec])
WPT	Wavelet packet transform (–)

Introduction

The growing demand for sustainable structures has brought increased attention to the field of structural health monitoring (SHM) in construction. SHM is a multidisciplinary field of engineering that uses innovative methods to monitor the safety, integrity, and performance of structures without disrupting their operation or performance. SHM can be divided into two main categories: non-destructive methods (NDM) and destructive methods. In recent years, much research has focused on NDM, as it allows for the assessment of the condition of the structure without altering it.

There are numerous techniques used in SHM, such as those based on acoustic emissions [10], vibration analysis [8], laser scanning [26], or ultrasonic waves propagation [25]. Acoustic emissions primarily result from the rapid release of energy from a localized source within a stressed material, which generates a transient elastic wave. These emissions can be caused by various fracture or deformation processes within the material, such as the initiation and expansion of cracks, separation at the microstructural level, and the movement of material phases [10]. On the other hand, the vibration analysis is depending on the amplitude of the sent signals to get valuable information on the state of the structure [8].

In recent years, there has been increasing interest in the use of ultrasonic waves for SHM. Previous research has shown that ultrasonic guided waves are effective for detecting and localizing damage in structures. For instance, a recent study by Rautela et al. [17] utilized ultrasonic guided waves and deep learning algorithms for damage identification in composite waveguides. Although our work uses a different method for SHM, the study done in [17] provides valuable insights into the potential of ultrasonic guided waves for damage detection. Another promising technique that uses ultrasonic guided waves to detect and locate damage in structures is the guided wave-based SHM. For example, a recent study by Nan Yue et al. [28] proposed a novel approach for using guided wave-based SHM to monitor large composite stiffened panels under varying temperature conditions. Their approach utilizes a building block (BB) method to conduct SHM analysis and associated tests at different



levels of structural complexity. Using data from lower-level structures in the proposed BB test scheme to higher-level structures, Nan Yue et al. were able to reduce the number of tests required for large and complex structures. Additionally, they proposed a two-step multi-damage localization method to detect and locate damages accurately. Their findings could be beneficial in developing more efficient and accurate guided wave based SHM systems for composite structures.

In the last decade, SHM has become an increasingly important area of research due to advancements in sensors, signal processing, and computing methods. One such development is a non-contact SHM system for machine tools, which has the potential to improve productivity and reduce costs by providing real-time monitoring of machining processes. In a study by Goyal and Pabla [7], a non-contact SHM system based on vibration signals collected through a low-cost, microcontroller-based data acquisition system was developed and tested on a vibration rig. The system was found to be cost-effective, reliable, and able to quickly measure vibration data without requiring alterations to the machine tool structure. The authors concluded that the system could effectively monitor the health of a machine and facilitate timely maintenance decisions.

Another emerging SHM technology is based on the use of the unmanned aerial systems (UAS) which provides a promising technology allowing for remote and non-destructive inspection of large-scale structures. However, real-time damage detection is crucial for efficient and effective maintenance of critical infrastructure. Recently, a vision-guided UAS with a lightweight convolutional neural network was developed by Jiang et al. to detect and locate bridge cracks, spalling, and corrosion in real-time [12]. The proposed system utilizes a stereo vision inertial fusion method for position data and an ultrasonic ranger to avoid obstacles, and a lightweight end-to-end object detection network for real-time edge computing during inspection. This system was successfully applied to a long-span bridge and demonstrated high accuracy and efficiency in detecting and locating damages. This recent technological advancement offers significant potential for enhancing the efficiency and effectiveness of structural health monitoring.

Most SHM techniques have been able to accurately detect damage in structures, but accurately locating the damage within large-scale structures remains a challenge due to the various factors that can influence its location, which is often difficult to detect. There were attempts done on 2D plates to localize existing damage with significant localization accuracy as done by Marković et al. [15].

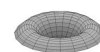
PZT impedance technique is a widely used approach in SHM for damage detection. A number of research studies have investigated the effectiveness of PZT sensors in detecting damages in concrete structures. For instance, in a study by Yang et al. [27], the sensitivity of PZT impedance sensors

for damage detection of concrete structures was evaluated. The study proposed using the structural mechanical impedance (SMI) extracted from the PZT admittance signature as the damage indicator and compared it to the traditional PZT electro-mechanical (EM) admittance as a damage indicator. The results showed that the SMI was more sensitive to damage, making it a better indicator for damage detection. The study also proposed a dynamic system to model the SMI and employed a genetic algorithm to search for the optimal values of the unknown parameters. These findings highlight the importance and potential of using PZT sensors for damage detection in concrete structures. Another study conducted by Vitola et al. [21] explored the use of a distributed PZT sensor system for damage identification in structures subjected to temperature changes. The methodology involved the use of multivariate analysis, sensor data fusion, and machine learning approaches to detect and classify damage in aluminum and composite structures. The experimental results showed that the methodology was successful in detecting and classifying damage despite temperature variations. This provides a prime example of the effectiveness of a distributed PZT sensor system in SHM applications.

Several research studies have explored the application of piezoelectric sensors for damage detection in different types of structures, such as bridges, buildings, and aerospace structures. For example, Fan et al. [6] used piezoelectric sensors to detect damage in a truss bridge and proposed an algorithm based on time-domain impedance responses acquired from the sensors. In another study, Jahangir et al. [11] proposed a method for detecting single, double, and triple damage scenarios in reinforced concrete beams using Wavelet transform coefficient as a damage index.

Damage identification is crucial in the maintenance of engineering structures, and various methods have been developed to achieve this goal. One promising approach is based on the wavelet packet transform (WPT). In a recent study done by Wang et al. [24], the authors proposed a novel index, the energy curvature difference (ECD), which is computed as the summation of component energy curvature differences after decomposing the signal using WPT. The ECD index was shown to be effective in identifying structural damage, even at low damage levels. The results suggest that the ECD index can complement existing methods and improve the accuracy of damage detection.

In recent years, Daubechies wavelets have become increasingly popular in various practical applications, particularly in the field of signal processing. These wavelets are well-known for their excellent properties of orthogonality and minimum compact support, making them useful for efficiently localizing non-regular zones in signals. Due to these properties, several studies have successfully used Daubechies wavelets for the numerical solutions of partial differential equations in structural mechanics as done by Díaz et al. [4]. In this



study, we have chosen to use the Daubechies wavelet due to its superior properties in wavelet analysis. As described in the comprehensive collection of wavelet transforms discovered by Walker [22], the Daubechies wavelet transform is defined in the same way as the Haar wavelet transform but with slightly longer supports, which provides a significant improvement in its capabilities. Another example of the application of Daubechies wavelet for damage detection can be found in the work of Guminiak et al. [9]. The authors used the discrete wavelet transform (DWT) in combination with the boundary element method to investigate damage detection in plates with defects. The signal function was decomposed using the Daubechies or Coiflet wavelet families, and the efficiency of DWT was studied in detecting damage. Their study conducted using the Daubechies 4 wavelet and Coiflet 6 or 12 wavelet families showed efficient results in detecting and localizing damage in plates with additional edges forming slots or holes, as well as the impact of measurement point distance on the efficiency of the method.

Another research exploring the use of wavelet transformations for detecting defects in structures was done by Knitter-Piatkowska et al. [14]. The authors applied a discrete wavelet transformation to detect defects in bridge trusses, with the family of Daubechies 4 wavelets being used. The analysis was performed on a 2D and 3D truss structure, and defects were modeled as local stiffness reductions in lower chord bars. The study found that wavelets are sensitive to bending effects of the truss' lower chord, but are impeded by the presence of vertical struts and diagonal bars. The method could detect more than one defect if they were located close to each other. However, the analysis revealed limited usefulness of DWT applied to study truss structures, as some defects could not be localized in the lower chord bars. Therefore, the authors suggest that while DWT can be an effective tool for detecting defects in simpler structures such as beams and plates, its applicability to truss structures may be limited. Further research was recommended to improve the effectiveness of DWT in detecting defects in truss structures.

The Daubechies wavelet has been widely used in various signal processing tasks, including compression, noise removal, image enhancement, and signal recognition. Thus, we use of Daubechies wavelets for analyzing signals acquired from specimens in both damaged and intact states to explore the potential of wavelet analysis for detecting and characterizing damage in structures. However, since the target structure of the investigated method is meant to be massive concrete structures, the choice of Daubechies 9 wavelet is made for the signal decomposition step as it offers a good balance between time and frequency localization, which can be important for processing large amounts of data efficiently. The Daubechies 9 wavelet has a longer support than Daubechies 4, which means it can capture more complex signal features with fewer

coefficients, reducing the computational complexity of the wavelet transform. Additionally, the Daubechies 9 wavelet has a higher order of vanishing moments than Daubechies 4, which means it can better preserve the smoothness of the signals being analyzed, even with noisy or coarse data. Furthermore, the calculation of the damage index based on the energy of each reconstructed signal from the approximation decomposition still yields a valid value compared to that obtained from the original signal. We conducted a comparison using higher-order Daubechies wavelets, which further confirms that the selected wavelet produces stable approximation contributions relative to the original signals.

The investigated method for damage detection proposed by Marković et al. [15] relies on having a reference state of the structure under consideration. However, calculating the loss of energy as a damage index involves comparing the examined and intact states of the structure, which may be influenced by various factors that could affect the applicability of the method. Hence, our work aims to optimize the method proposed by Marković et al. [15] by thoroughly exploring all potential factors that could impact its performance. We attempt to achieve this optimization by systematically testing different parameters and evaluating the resulting outcomes. All the investigated parameters of this work are determined based on the recent researches presented here and on the thorough study of the investigated method. The aim of this work is to provide an effective and relatively computationally cheap method for evaluating complicated techniques within the field of SHM.

In this paper, the damage detection hybrid method suggested in our previous research.

[3, 15] is further investigated and the study is extended to improve the feasibility of the method and increase the accuracy of the damage detection and its localization. A detailed example of applying the method to a 2D concrete plate is provided. Two models representing the intact and damaged states of the specimen are investigated in numerical simulation. The first parameter of interest is the ToF criterion used within the hybrid method. Further investigation is applied to recorded signals where various truncation strategies are applied to determine their impact on damage detection accuracy. Additionally, the impact of the number of PZTs used in the numerical experiment is also examined.

The structure of this paper is organized as follows. The introduction section highlights the growing demand for sustainable structures and the increasing attention to the field of SHM in construction. The methodology section outlines the damaged index for damage detection, the concept of the hybrid method, and the effect of ToF on the damage index calculation. The numerical simulation section presents the model inputs and characteristics, as well as the investigations conducted, which include the time of flight criteria, truncation policies of signals, signals enhancement strategies, and the number



of added PZTs for damaged localization. The results section showcases the findings of the applied investigations, such as the comparison between applied ToF criteria, detected damage for the truncation at a specific time, the detected damage for the truncation at ToF plus the excitation signal duration, the detected damage for the truncation at ToF, and the effect of the modification strategies and the number of PZTs. Finally, the conclusion and recommendations section presents the major contributions of this paper and provides suggestions for the future research in this field.

Methodology

This paper provides a broader insight into the methodology proposed in [3, 15], and identifies options for the enhancement of the damage localization accuracy. The relationship between the distribution of the PZTs within the specimen and the structural element length is investigated. Additionally, the impact of the length of the signal being analyzed on the calculation of the damage index is studied by applying various truncation techniques to the recorded signals.

Damage Index for Damage Detection

To calculate the one-dimensional damage index, the energy difference between the undamaged and damaged states of the specimen is determined using the root mean square deviation (RMSD) method [15]. This difference is calculated by decomposing the input signal into 2^n sets using n -level wavelet decomposition, with the mother wavelet being the Daubechies wavelet db9. The motivation for selecting this particular mother wavelet is due to its ability to effectively localize signal features and exhibit regularity properties [14]. These attributes make it well-suited for analyzing signals containing discontinuities and spikes.

The energy of a single wave form from one sender to one receiver is then calculated from each of these decomposed signals.

$$X_S = \{X_1, X_2, \dots, X_j, \dots, X_{2^{n-1}}, X_{2^n}\} \quad (1)$$

$$X_j = [x_{j,1}, x_{j,2}, \dots, x_{j,m}] \quad (2)$$

The vector X_S in Eq. (1) contains the decomposed signals, which are at a total of 2^n levels, and the vector X_j is one of the decomposed signals with a total of m sampling data.

Subsequently, the energy of each decomposed signal can be calculated as:

$$E_{(),k} = X_{k2}^2 = x_{k,1}^2 + x_{k,2}^2 + \dots + x_{k,m-1}^2 + x_{k,m}^2 \quad (3)$$

where k refers to the decomposed signal for which the energy is being calculated ($k = 1, \dots, 2^n$). As a result, the energy of

each state of the specimen (h : intact, d : damaged) can be represented in the following two vectors:

$$E_d = E_{d,1}, E_{d,2}, \dots, E_{d,2^n} \quad (4)$$

$$E_h = E_{h,1}, E_{h,2}, \dots, E_{h,2^n} \quad (5)$$

where each of these vectors includes the energy of each decomposition of the corresponding state. After that, using the RMSD rule, we can calculate the damage index as follows:

$$DI = \sqrt{\frac{\sum_{p=1}^{2^n} (E_{d,p} - E_{h,p})^2}{\sum_{p=1}^{2^n} E_{h,p}^2}} \quad (6)$$

It is important to note that the damage index ranges from 0, indicating an undamaged specimen, to 1, indicating a fully damaged specimen.

The Concept of the ToF and Energy Dependent Hybrid Method

The goal of the investigated method is to identify and locate damage in two-dimensional concrete elements by acquisition of the waveforms from the PZTs used as sources and receivers of the waves propagating through the elements. The paper analyzed the influence of the arrangement and number of PZTs to damaged detection accuracy.

The method depends on both the signal energy and the ToF criteria of the corresponding signal. The algorithm of the method was initially proposed in [15] and is summarized in Fig. 1.

The left-hand side of the figure includes the main steps which are the distribution of the PZTs on the surface of the observed element, sending of excitation signals from each of the PZTs iteratively and recording its response at all other PZTs. Finally, the recorded signals are decomposed and processed so that the corresponding energy is calculated in both states of the specimen (intact / damaged). This results in the calculation of the damage index for each actuator–sensor path (AS-path).

The right-hand side of the figure will not be analyzed in this study, but it is important to note that the applied interpolation introduces some errors in damage localization. Additionally, the visualization of the results is done using a contour plot function, which applies linear interpolation by default. These post-processing steps should be taken into consideration for future improvements.

A summary of the interpolation step applied in the investigated method is presented in Fig. 2, where the damage index matrix is generated from the acquired signals of both intact and damaged cases of the specimen and each value within the matrix refers to the 1D damage index value at the corresponding actuator–sensor path (AS-path).

Fig. 1 The algorithm of the ToF and energy dependent hybrid method [15]

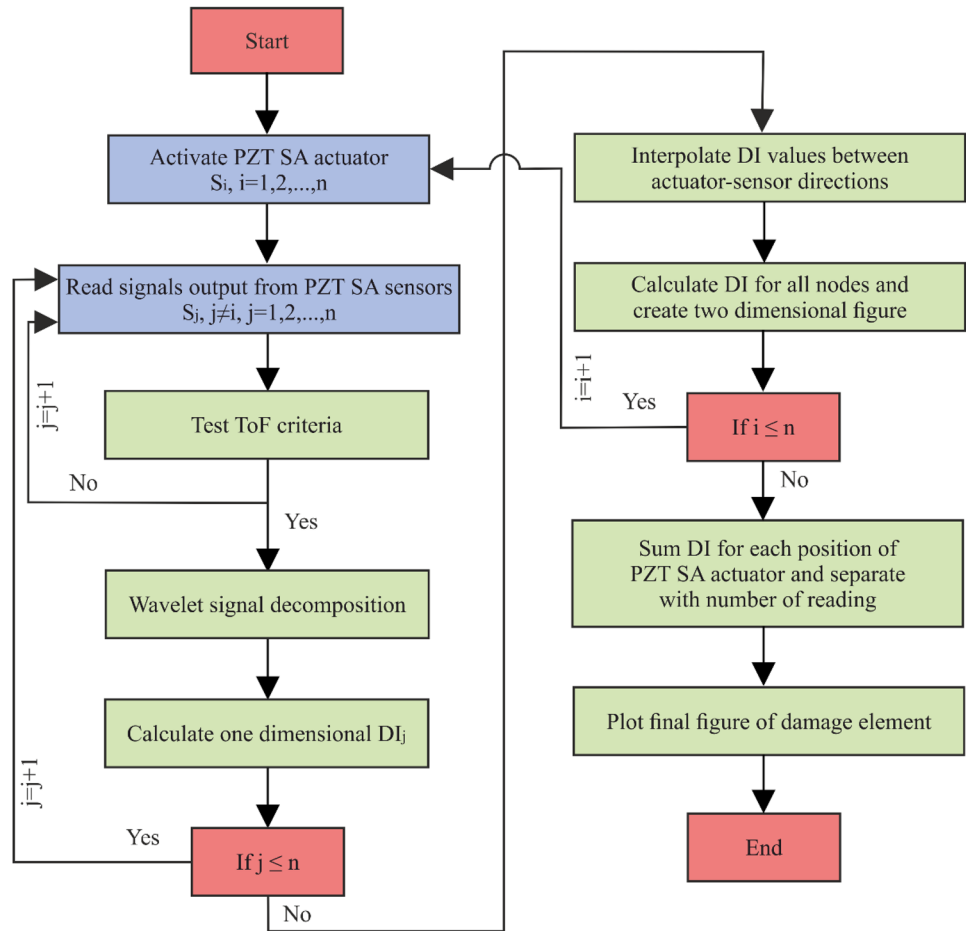
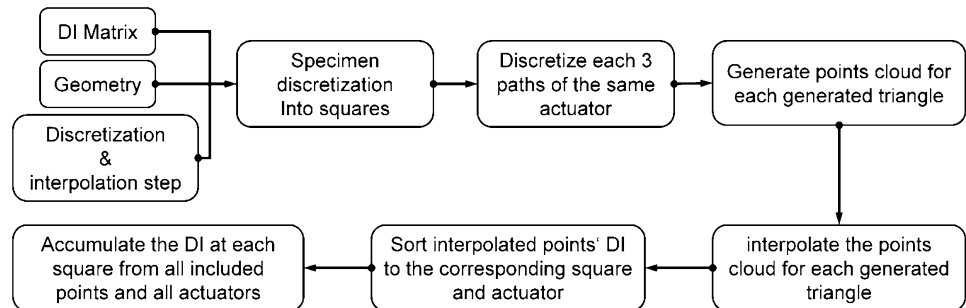


Fig. 2 The DI interpolation flowchart of the ToF & energy dependent hybrid method



To start the interpolation of this matrix, the specimen is discretized into squares. After that, each three AS paths ($A_i - S_j, A_i - S_k, A_i - S_l$) related to the same actuator are discretized as shown in Fig. 3. Correspondingly, for each discretized point on those paths, a triangle is generated. A cloud of interpolation points is generated for each of the generated triangles. Finally, each interpolation point within the generated cloud is interpolated according to the DI surface of the corresponding triangle. It is important to notice that each corner of the generated triangles has the DI value of the corresponding AS-path.

The Effect of ToF on the Damage Index Calculation

As previously mentioned, the hybrid method relies on determining the ToF which is used for the calculation of the 1D damage index. The ToF plays a decisive role in the hybrid method. Yet according to the authors' best knowledge a systematic guidance or recommendation for the selection of the ToF criteria is still missing. Therefore, three different ToF criteria and their influence to damage detection are investigated in details in this work.

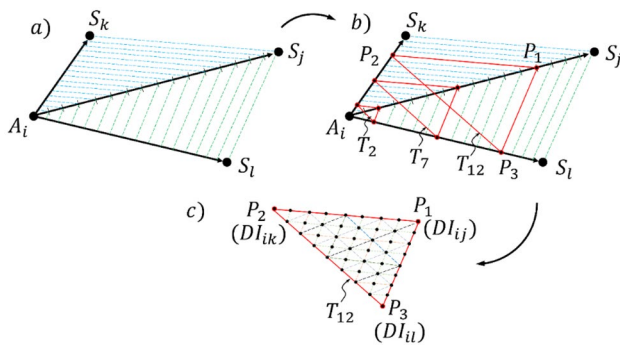


Fig. 3 Generation of the interpolation points of each triangle; **a** discretization of three AS-paths, **b** Generation of triangles of the discretized points, **c** generation of the interpolation points cloud of each triangle

1. Threshold of the max amplitude

The ToF is defined here as the point of time at which the amplitude of the signal is reaching a value that is equal to a specific percent threshold value (5%) of the maximum amplitude of the signal within the analyzed time. It is important to mention that this method is very dependent on the considered analyzing time of the signal and also the purity of the recorded signals. For easy referring of this ToF criterion, it will be referred as ToF1

2. First zero crossing

In this method the ToF is determined as the time of the first datapoint of the signal that has an amplitude not equal to zero. This criterion will be abbreviated by ToF2 in this work

3. The P-phase time of the signal energy

The third ToF criterion in this work is denoted as ToF3. The determination of the ToF according to this criterion is based on the algorithm for the automatic P-phase arrival time picker proposed by Kalkan [13] and implemented in MATLAB libraries [5], which finds the onset of the P-phase by tracking the power of the damping energy. This method was also implemented in [18] for the detection of ToF of signals propagated within thin-walled structures with considerable accuracy

Investigation Strategy

The research concentrates on investigating the specifications with missing recommendations in the hybrid method by applying series of targeted simulations that include different possible values and policies for those specifications.

The investigated specifications are:

- The type of ToF criteria used for the ToF test of its algorithm
- The effect of PZTs number used for the damage detection
- The exact length to be considered for each recorded signal

The evaluation of each investigation is done by comparing the Euclidean-distance (ED) between the center of detected damage and the real center of existing damage. This work presents an oriented strategy for evaluating the contribution of each parameter to the method of interest. The strategy starts similarly to the Taguchi method by specifying the target function, which is to minimize the ED between the real and detected center of damage. Furthermore, the parameters of interest and their corresponding levels are specified, as shown in Table 1. In the table the levels denote the ToF criteria ToF1, ToF2, and ToF3 referred to as in Sect. 2.3. Similarly, the levels of the truncation position refer to the time where the signals are truncated for the energy loss calculation between the intact and damaged cases. Additionally, the truncation at each of ToFi and ToFd refers to the truncation at the ToF of the specimen in the intact state and the ToF of the specimen in the damaged state. An additional time duration for truncation is added to the ToF in two levels with a magnitude equal to the excitation wave duration (WD). The investigation strategy applied in this study is summarized in a flowchart presented in Fig. 4.

The next step of the investigation starts with choosing one parameter and followed by examining all its levels in relation with one level of each of the other parameters. An evaluation step is applied after that to choose the best level of this parameter to be used in the next round which will examine another parameter with all its values which is not tested yet.

Table 1 Parameters and levels of the investigation strategy

Factors/Parameters	Levels
Used ToF criteria	no ToF, ToF1, ToF2, ToF3
Truncation position	no truncation, at fixed time, at ToFi, at ToFd, at ToFi + WD, at ToFd + WD
Number of PZTs	12, 16, 20

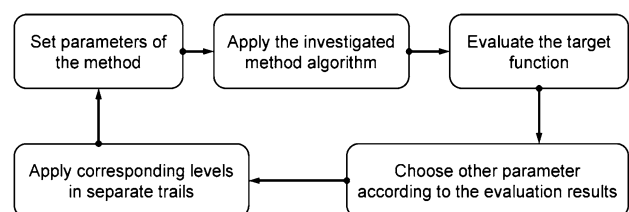


Fig. 4 Flowchart of the investigation strategy

Table 2 Applied trails for the investigation strategy

Trail	Factors/Parameters	Fixed value 1	Fixed value 2	Values of investigated levels
1,2,3,4	Used ToF criteria	16 PZTs	no Truncation	no ToF, ToF1, ToF2, ToF3
5,6,7,8,9,10	Truncation position	16 PZTs	ToF3	No truncation, at fixed time, at ToFi, at ToFd, at ToFi + WD, at ToFd + WD
10,11,12,13,14,15	Number of PZTs	ToFi, ToFd	ToF3	12 PZTs, 16 PZTs, 20 PZTs

Table 3 Material properties of concrete

Young's modulus [GPa]	30
Poisson's ratio	0.1
Density [kg/m ³]	2400
α (damping coefficient)	2058.23
β (damping coefficient)	1.105×10^{-8}

Using this method saves a lot of tests to reach a suitable value of the target function. In Table 2, a total of 18 testes are listed to present all attempts applied in this research.

Three other attempts are built on the results of all these attempts to get a better performance from the investigated method. These attempts will be described in details in the next chapter.

Numerical Simulation

Two specimens of a 2D concrete plate are modeled as a linear elastic material with the dimension of $0.4 \times 0.4 \times 0.04$ [m]. The software used for the numerical simulation is ABAQUS/ EXPLICIT. One of the models is built to refer to the concrete plate in its intact state so that its results will be used in the hybrid method for the calculation of the damage indices, while the other model refers to the damaged case of the concrete plate. Both models will be used in a hybrid method to calculate damage indices. The models will be processed according to the steps outlined in the hybrid method algorithm. However, the process of damage index calculation, the interpolation of DI at points between the AS-paths, and visualization of the damage detected are done using MATLAB code.

Models Inputs and Characteristics

The Material Properties

Both models in the research use the same material properties for the concrete, which are presented in Table 3.

The values of the Rayleigh damping coefficients α and β are selected according to the recommendations from literature [19] where the direct pitch-catch model is used. This

model involves sending a pulse through the material and measuring the response at two sensors located on either side of the pulse. By analyzing the decay of the pulse signal as it travels through the material, the damping factors can be determined [20]. This method is commonly used in the field of non-destructive testing to assess the condition of materials and structures. The complete procedure of calculating the damping coefficients where thoroughly presented by Tian et al. in the research [20]. In the following paragraph, a short summery is presented.

Determination of Rayleigh Damping Coefficients

The Rayleigh damping model is widely used due to its ease of implementation and the ability to decouple the dynamic equations. The relationship between mass and stiffness in Rayleigh damping can be expressed as follows [1]:

$$\mathbf{C} = \alpha \mathbf{M} + \beta \mathbf{K}, \quad (7)$$

where \mathbf{C} is the damping matrix and the equation is called the Rayleigh damping, after the founder of its use Lord Rayleigh. \mathbf{M} and \mathbf{K} are the mass and stiffness matrices respectively. The coefficients α and β are the proportionality constants for the mass and stiffness damping, respectively.

The damping ratio ξ can be calculated using the following formula [1]

$$\xi = \frac{\alpha}{2\omega} + \frac{\beta\omega}{2}, \quad (8)$$

where ω is the angular frequency of the system and is equal to $2\pi f$, and f is the frequency. Providing that the vibration of the structure follows the logarithmic attenuation law, the ratio of vibration amplitudes between one cycle and n cycle of vibration can be described as [20]:

$$\ln \left(\frac{u}{u_n} \right) = \frac{2n\pi\xi}{\sqrt{1 - \xi^2}} \quad (9)$$

Due to the fact that the damping ratio is a very small number and its square is much smaller, the denominator can be considered equal to 1, hence Eq. (9) will results in the following [20]:

$$\ln \left(\frac{u}{u_n} \right) = 2n\pi\xi \quad (10)$$

To better understand the behavior of an elastic mechanical wave, the amplitude at different distances from the actuator to two arbitrary reference positioned sensors l_1 and l_2 can be considered. The amplitudes at distances l_1 and l_2 are denoted as A_1 and A_2 , respectively. The time it takes for the wave to travel from the actuator to the sensor at distance l_1 and l_2 are defined as t_1 and t_2 , respectively. Thus, a relationship between the wave propagation distance Δl and the time interval t_{int} can be established using the following equation [20]:

$$t_{int} = t_2 - t_1 = \frac{\Delta l}{C_L} = \frac{l_2 - l_1}{C_L}, \quad (11)$$

where C_L represents the longitudinal wave propagation velocity. Furthermore, the peak amplitude at the second sensor A_2 can be calculated with respect to the peak amplitude of the first sensor A_1 by making use of the absorption attenuation coefficient of the mechanical elastic wave k_ω as follows [23]:

$$A_2 = A_1 e^{-k_\omega \Delta l}, \quad (12)$$

Alternatively, the previous equation can be rewritten as:

$$\ln \left(\frac{A_2}{A_1} \right) = k_\omega \Delta l, \quad (13)$$

To make Eq. (13) equivalent to Eq. (10), it is enough to pick the reference position which corresponds to the position of the actuator in such a way that t_{int} can be expressed as the product of the number of cycles (n) and wave period ($T = 1/f$), and substituting the same in Eq. (11). This is done with the assumption that the attenuation of vibration and the wave propagation take place due to the material damping. Knowing that the absorption attenuation of the mechanical elastic wave is equivalent to the logarithmic decrement, Eq. (10) and Eq. (13) are equal as follows [16]:

$$2n\pi\xi = 2 \left(\frac{f\Delta l}{C_L} \right) \pi\xi = k_\omega \Delta l, \quad (14)$$

$$k_\omega = \frac{2\pi f\xi}{C_L} = \frac{\omega\xi}{C_L} = \frac{\omega}{C_L} \left(\frac{\alpha}{2\omega} + \frac{\beta\omega}{2} \right) = \frac{\alpha}{2C_L} + \frac{\beta}{2C_L} \omega^2 \quad (15)$$

To determine the damping factors using the direct pitch-catch model, a set of two PZTs are used to excite and receive signals from the structure. The PZTs are placed on the surface of the structure and the damping

factors are calculated based on the time delay between the two received signals. Measuring the amplitudes for different excitation frequency, enables us to generate a fitting curve for the relation between k_ω and ω . Finally, the curve equation leads to the calculation of both damping factors.

The Excitation Signal

Both models are excited with the same function which represents an external force defined as a 3.5-cycle Hanning-windowed tone burst:

$$P(t) = \begin{cases} \left[1 - \cos \left(\frac{2\pi}{N} t \right) \right] \sin(2\pi f t), & \text{for } 0 \leq t \leq \frac{N}{f} \\ 0, & \text{for } t > \frac{N}{f} \end{cases} \quad (16)$$

where f signal frequency (in the model 100 kHz) N number of cycles (in the model 3.5 cycles) t time (duration of the signal) (in the model 3.5×10^{-5} s) $P(t)$ the excitation by the actuator.

The high frequency of 100 kHz is chosen because it can detect small defects in the concrete structure and it eliminates the ambient noise that may interfere with the detection of defects. The thing that makes it easier to isolate and analyze the signal from the concrete specimen.

The ABAQUS/EXPLICIT package was used to perform the analysis, employing C3D8R eight-node prismatic finite elements with reduced integration and Hourglass control.

Applied Investigations

In this research, a series of investigations are applied to gain a better understanding of how to accurately locate existing damages in concrete structures.

The Time of Flight Criteria

As mentioned in the previous section, three criteria are considered to see its effect on the accuracy of the damage localization.

Truncation Policies of the Signals

The damage detection applied by the hybrid method depends on the energy loss which is calculated from each recorded signal. The signals resulting in the numerical models are analog signals which give great importance to how many datapoints does each signal have. Thus, the energy computation demands an equal number of data points for each signal path between the intact and damaged cases of the specimen.

However, the signals acquired at each sensor are dependent on the time increment and the analysis time. Furthermore, dealing with a propagated excitation wave that is faster than the analysis time results in recording additional reflected waves from the boundaries of the specimen. This was the trigger for applying different truncation policies on the signals to see its effect on its energy change and consequently on the damage localization. The applied truncation policies are listed as follows:

- Truncation at specific time

In this policy, the truncation is applied for all signals at all paths at a specified time where the longest path signal arrived at its sensor in addition to two reflected phases of signals. This was observed in our case at the time ($t = 2.24 \times 10^{-4}$ s) with a total of 8000 data point. This is applied for both intact and damaged cases to get the damage index values of each AS-path.

- Truncation at the ToF of each signal + duration of the excitation wave:

The duration of the excitation signal is added to the ToF of each signal at each path in this attempt. The aim was to see whether the energy of the complete signal being recorded at the sensor will contribute to the damage localization and also to avoid considering the reflected signals from the boundaries being recorded at each sensor.

- For this truncation, we had two possibilities of application which are:

A. Considering the ToF at the intact case for the truncation of signals of each path in both the intact and damaged cases of the specimen.

B. Considering the ToF at the damaged case for the truncation.

- Truncation at the ToF of each signal

In this strategy, only the data points of each signal until the ToF of the corresponding signal are considered. However, as in the previous policy, truncation is applied considering the ToF of the intact case at one attempt, and the ToF of the damaged case as a second truncation possibility.

Signals Enhancement Strategies

As an extended attempt to enhance the efficiency of the hybrid method, the recorded signals of each sensor are post-processed to reduce or delete the misleading components.

In the following paragraphs, two techniques are presented. The first one depends on extending the simulation space to remove reflected signals at the boundary, while the second one sets the amplitudes of signals of the intact case between their Time of Flights (ToF) in the intact case and the damaged case to zero.

- Extending the space of simulation model

This strategy is applied to get rid of the reflected signals from the boundary of the models of both intact and damaged cases. The goal is to obtain pure signals at each sensor to provide valuable information about the change of energy and achieve better localization of the damage.

Figure 5 shows the extension applied at each edge of the 2D concrete plate. The length of the extension is determined based on the material property and the excitation wave velocity to ensure that the reflected signal is not recorded at the sensor within the analysis time. The time (t) needed for a signal to travel back to the sensor from the extended boundary should be long enough to prevent the reflected signal from interfering with the recorded signal.

- Modification of intact case signals

In this attempt, the signals of the intact case are post-processed in such a way that their amplitudes between the ToF corresponding to the intact case and the corresponding ToF of the signal on the same path at the damaged case are set to zero, see Fig. 6. This was considered to reduce the amplitude change of the signals in the intact case after

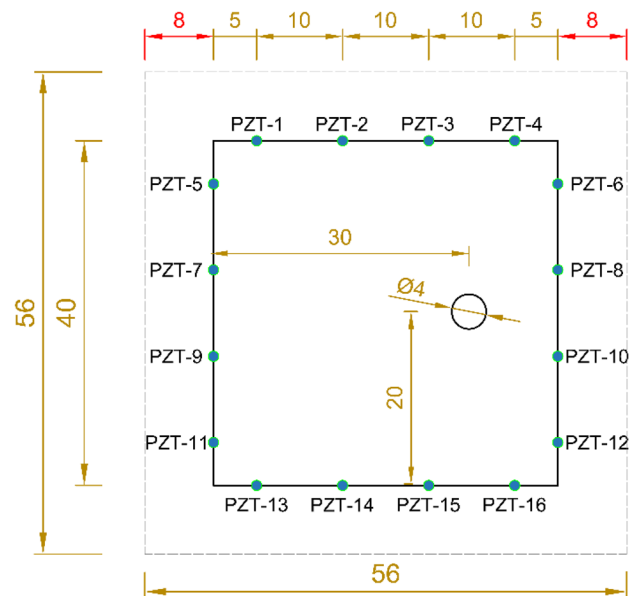


Fig. 5 Extended space of the simulation



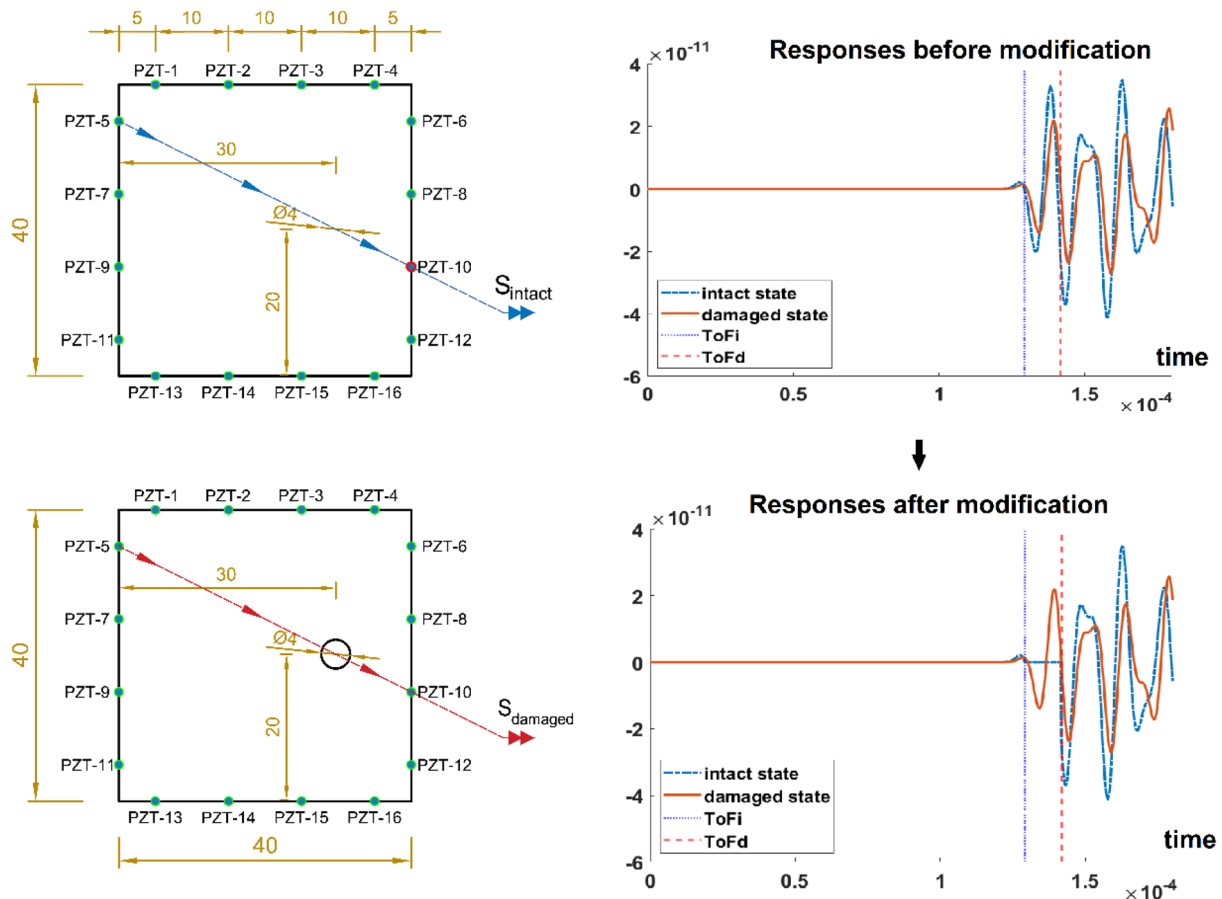


Fig. 6 Intact signal modification between ToFi and ToFd

their arrival at the sensor. Thus, controlling the change of energy between the intact case and the damaged case after arrival at each sensor.

The Number of Added PZTs for Damage Localization

The relationship between the number of PZTs and the mesh-size used for the simulation is investigated. Consequently, the more PZTs are used, the fewer elements are used between each PZT. This effect the accuracy of the final interpolation process of the hybrid method.

Most of the experiments were executed using 12, 16, and 20 PZTs distributed equally on the boundary of the specimen. However, an additional attempt is applied by increasing the number of PZTs explicitly between the PZTs with the greatest damage index values on each edge. See Fig. 7. In this technique, ten extra PZTs were added on each edge of the specimen between two PZTs with the greatest damage index value. The aim is to increase the accuracy of the damage localization with a minimal number of additional PZTs.

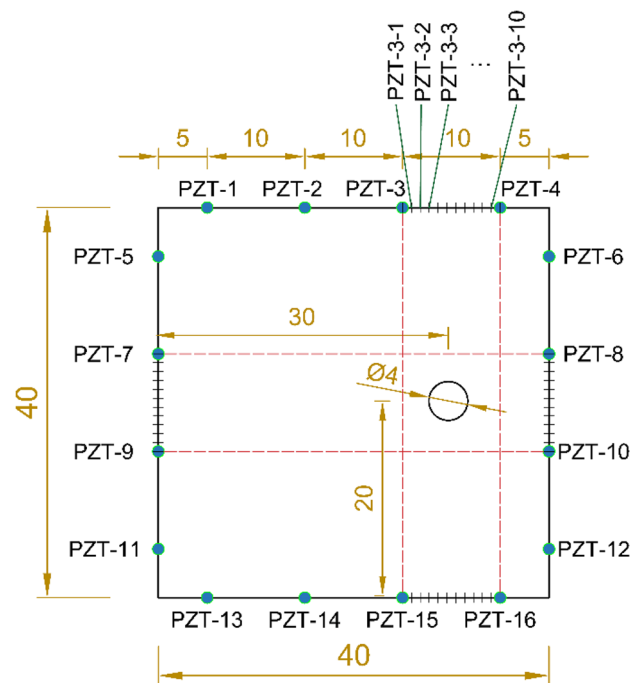


Fig. 7 PZTs addition policy to increase damage localization

Results

In this section, all the simulation results are presented. Firstly, the effect of the ToF on damage localization will be covered. After that, the truncation policies applied on the recorded signals and the applied modification are discussed. Finally, the effect of the number of PZTs used for damage detection presented.

All models presented in the following paragraphs have the same time increment (2.8×10^{-8} s) and a mesh size of

(0.00105 m) that satisfies the critical conditions of time increment and mesh size presented in [2].

Comparison Between Applied ToF Criteria

In this attempt, a complete duration of (2×10^{-3} s) for all signals is considered for the calculation of the damage index. In Fig. 8, a comparison between the resulted damage location in case of no ToF criteria was considered and the case of considering the threshold ratio “ToF1”, First Zero Crossing “ToF2”, P-Phase “ToF3” ToF criteria, respectively.

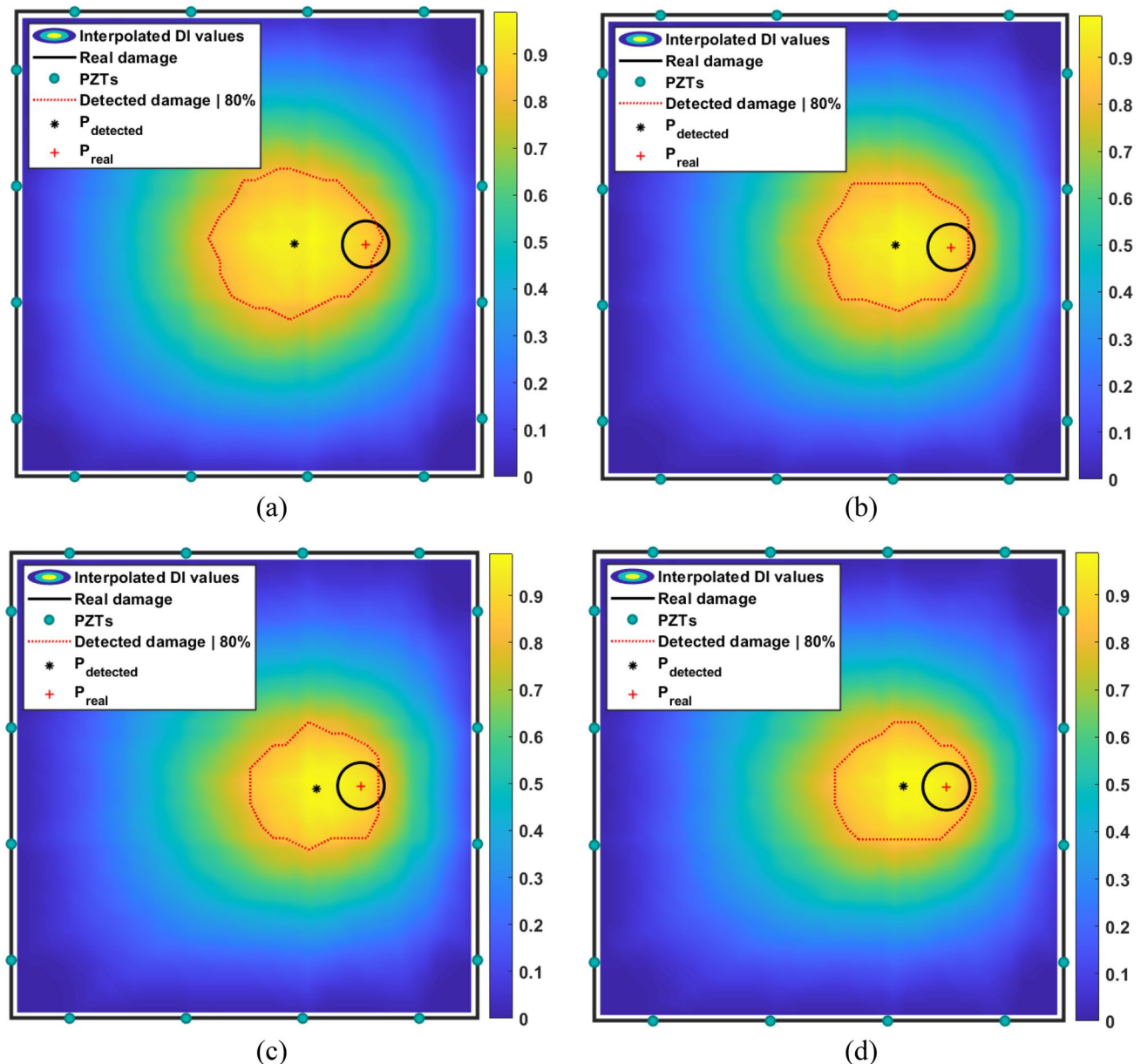


Fig. 8 Investigating the ToF criteria for the damaged localization; **a** no ToF criteria is considered, **b** applying the ToF1 criteria, **c** applying the ToF2 criteria, **d** applying the ToF3 criteria

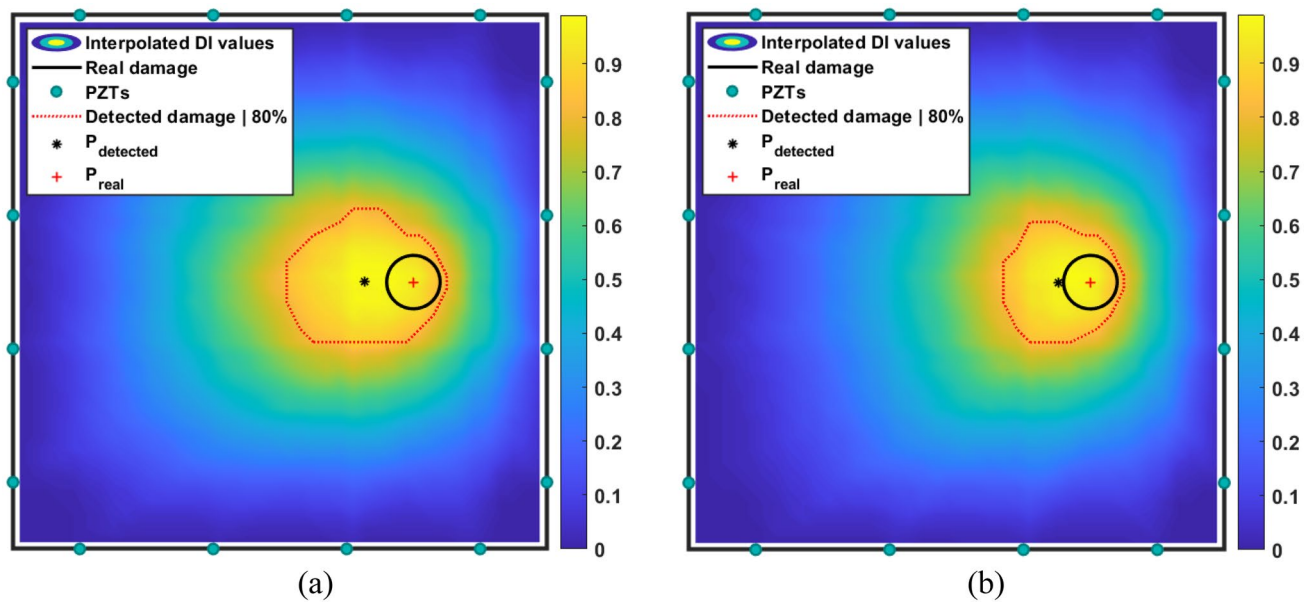


Fig. 9 Damage localization with fixed time truncation for all signals; **a** no truncation applied, **b** with truncation after a fixed number of datapoints (8000 datapoint)

In the previous figure, the red-dotted line refers to the detected damage area when only considering the points where their DI values are greater or equal to 80% of the maximum value of DI recorded in the numerical experiment.

From this comparison, it is clear that the use of ToF in the hybrid method is adding some improvement to the damage localization. However, the accuracy of the results is still not enough.

Truncation of Signals

Since the use of complete signals in the previous attempt was not enough convincing, the signals are truncated here according to different considerations presented in the following paragraphs.

Detected Damage for the Truncation at a Specific Time

As a first truncation policy, all the signals in both intact and damaged states of the specimen are truncated at a fixed time, Fig. 9. The choice of that time is done simply to cover the duration of the excitation wave travel on the longest path within the specimen in addition to the excitation wave duration with some additional margin. The idea behind that is to see whether this part of the signals is sufficient to get a better damage localization.

From this attempt, it is noted that the truncation has already added a good improvement on the damage

localization since the center of the red area of the detected damage is moved toward the real damage location.

Detected Damage for the Truncation at ToF Plus the Excitation Signal Duration

As a second truncation policy, the ToF is used to apply truncation. The truncation is applied to the signals of each AS-path at the ToF of its signals plus the excitation signal duration. Two truncation possibilities are available: one using ToFi and the other using ToFd for truncation, see Fig. 10.

From this comparison, it is noticed that this policy of truncation did not achieve better performance than the previous attempt. This means that the considered truncation point is not suitable yet.

Detected Damage for the Truncation at ToF

In this attempt, truncation is applied at the ToF of each signal. Again, there are two truncation possibilities, similar to the previous attempt. The ToF criteria used for this attempt is the P-phase criteria, abbreviated as ToF3 in this work. This criterion was chosen due to its high accuracy in detecting the damage in the previous trial results, Fig. 11

Removing the datapoints after the ToF of each signal leads to a greater enhancement in the damage localization since the center of the detected damage is moved more to the center of the real damage.

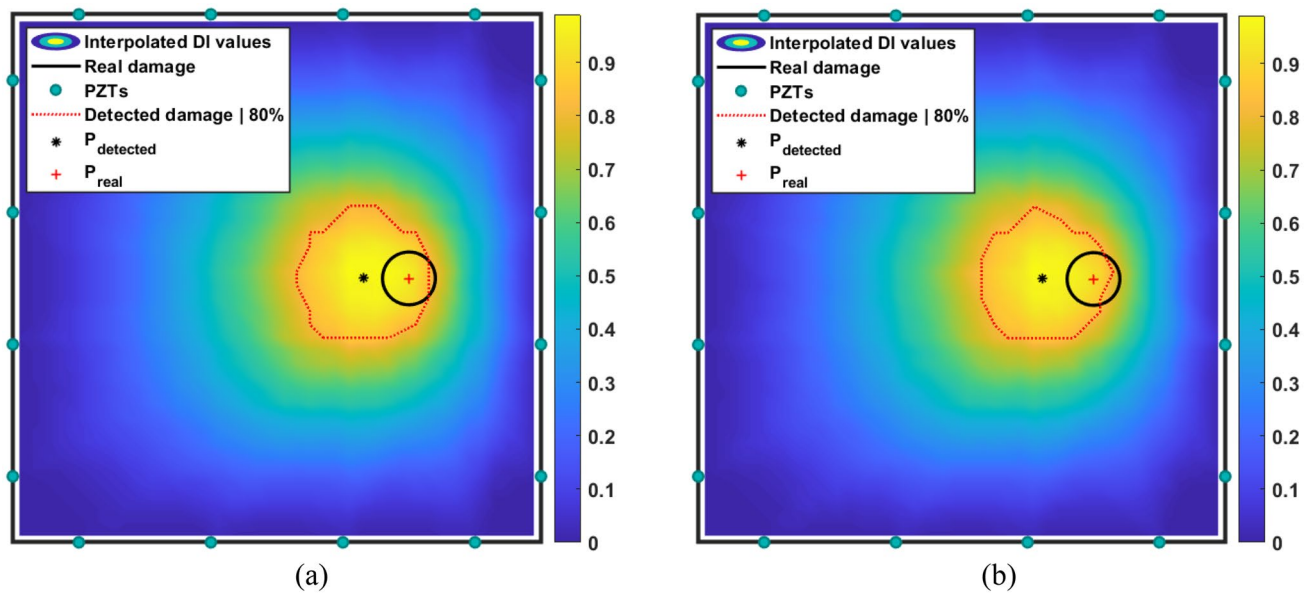


Fig. 10 Damage localization with truncation policy of signals **a** at the ToFi + WD, **b** at the ToFd + WD

However, removing the damage index values of the AS-paths located on the boundary of the specimen does not result in better localization of the damage, see Fig. 12.

Results of the Modification Strategies

In this section, the localization results of the modification strategies are presented. The first strategy involves extending the model space to prevent reflected signals from reaching

the sensor of interest. The second modification builds on the first by modifying the intact-state signals of the extended models. Similar to the previous trial, ToF3 is used for ToF calculation in both attempts. The modification results of both attempts are presented in the following figure.

In these attempts, a finer mesh size of (0.0007 m) is used to determine whether there is a loss in damage localization due to the mesh size.

Both modification strategies are applied with signal truncation at the ToFd. However, both attempts presented

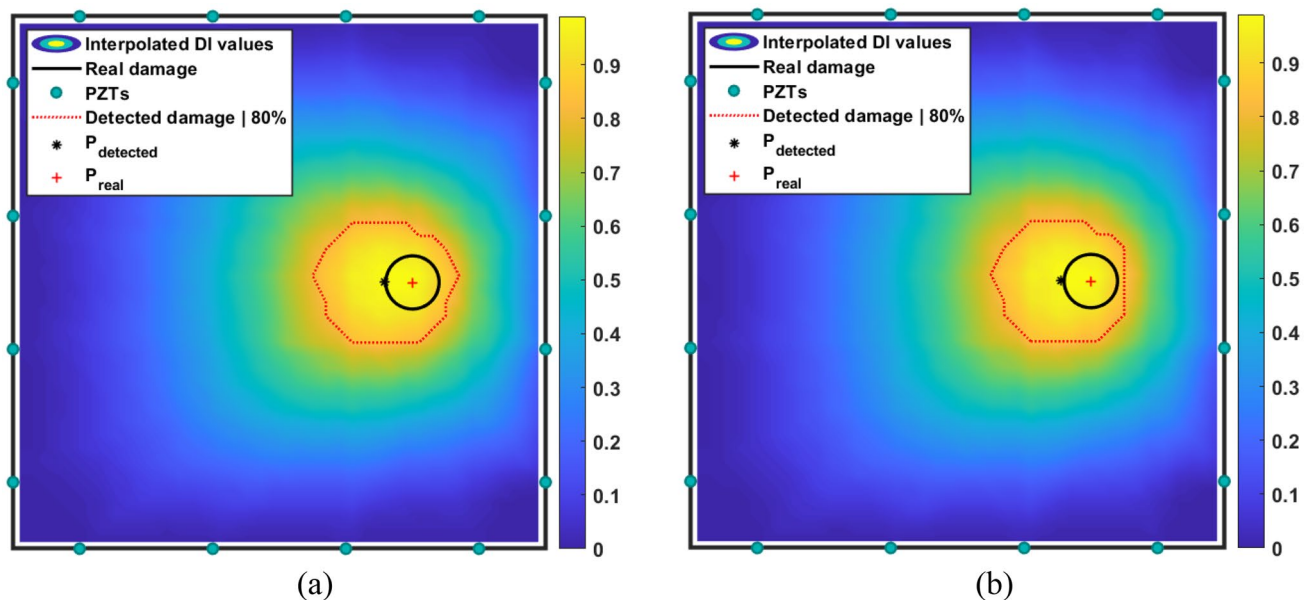


Fig. 11 Damage localization with truncation at the ToF of each signal **a** at ToFi, **b** at ToFd

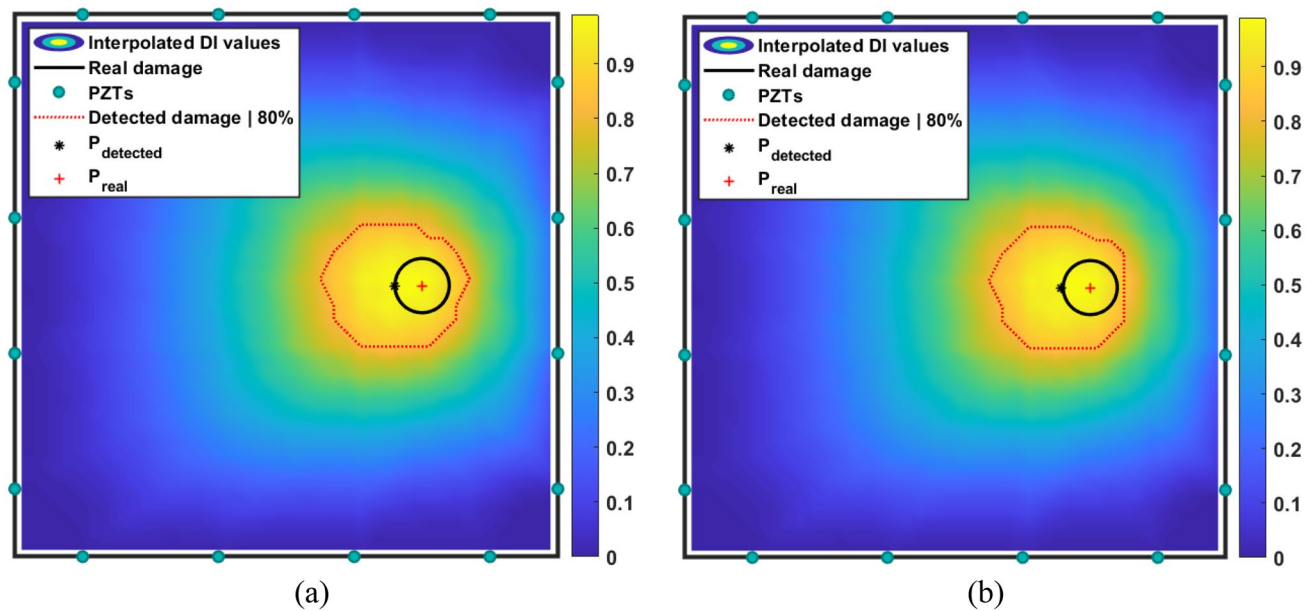


Fig. 12 Damaged localization with truncation at the ToF of each signal and removed DI values of the boundary AS-paths; **a** truncation of signals at ToFi, **b** truncation of signals at ToFd

in Fig. 13, show no improvement in the performance of the hybrid method. On the contrary, the accuracy is reduced compared to the previous attempts. This leads to the conclusion that the use of a finer mesh size does not match the other used parameters, especially, the number of PZTs.

Effect of the number of PZTs

In this section, we explore the effect of the number of PZTs on damage localization when truncation is applied at the ToFd of the signals of each AS-path. We tested the damage localization performance using 12, 16, and 20 PZTs, and the results are presented in Fig. 14.

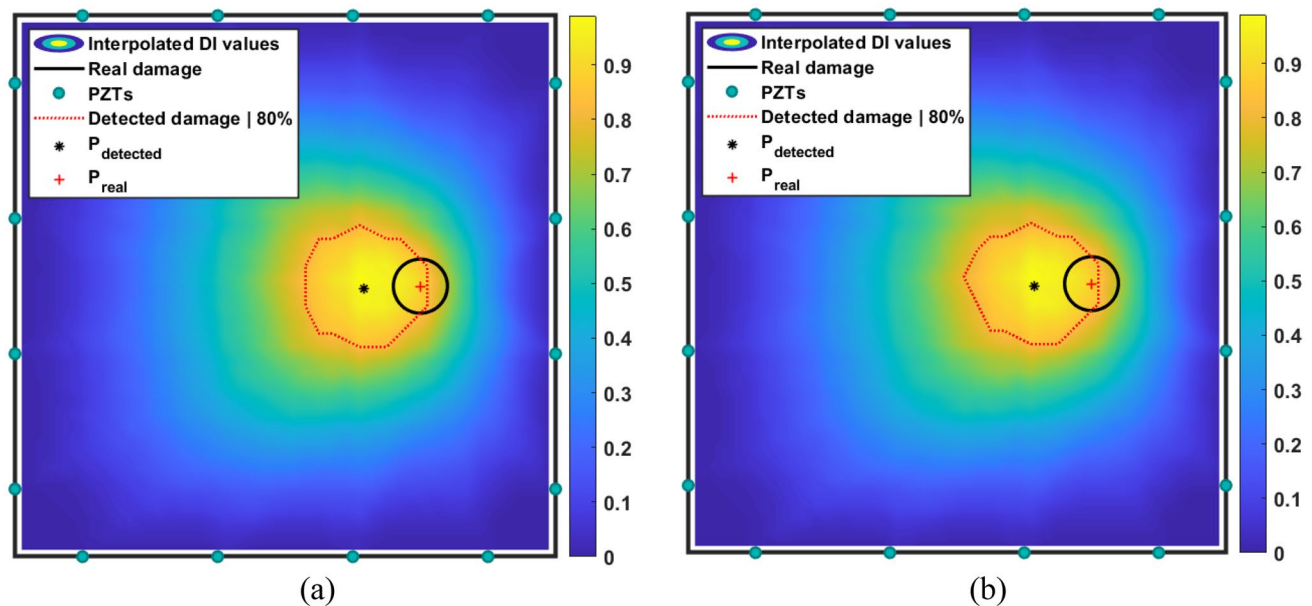


Fig. 13 Damage localization of the modification strategies with the extended model; **a** extended geometry, **b** extended geometry with modified signals

Based on the previous figure, it is clear that using 12 or 20 PZTs results in better performance than using 16 PZTs. However, these results do not provide a definitive rule for selecting the appropriate number of PZTs for future studies or models. Further investigation is necessary to determine the optimal number of PZTs for different scenarios and configurations.

On the other hand, considering the truncating signals at the ToFi, the resulting localization of damage is relatively changed as shown in Fig. 15.

It is noteworthy that using 12 PZTs results in very accurate damage localization, while using more PZTs, such as 16 or 20, results in relatively good localization, but not better than using 12 PZTs. These findings suggest that there may be a conflict between the number of PZTs, the mesh size used in our simulation, and the interpolation

element size used in the hybrid method. To address this issue, an extended improvement policy is applied by adding 10 PZTs on each side of the specimen, between the old locations that include the detected damage position of the previous attempt, as shown in Fig. 7. This iterative method improves the accuracy of damage localization with a minimal addition of PZTs, as shown in Fig. 16.

The figure presented shows three lines, each corresponding to a different filter value used to detect the damage. The red “dotted-line” represents the detected damage with a damage value greater than or equal to 80% of the maximum detected damage index value. The “dash-dot” black line corresponds to the detected area with a filter of 90% of the maximum DI. By assigning the filter to 95% of the maximum DI, we get the “dashed-line” in blue, which corresponds to the most accurate localization of the detected damage.

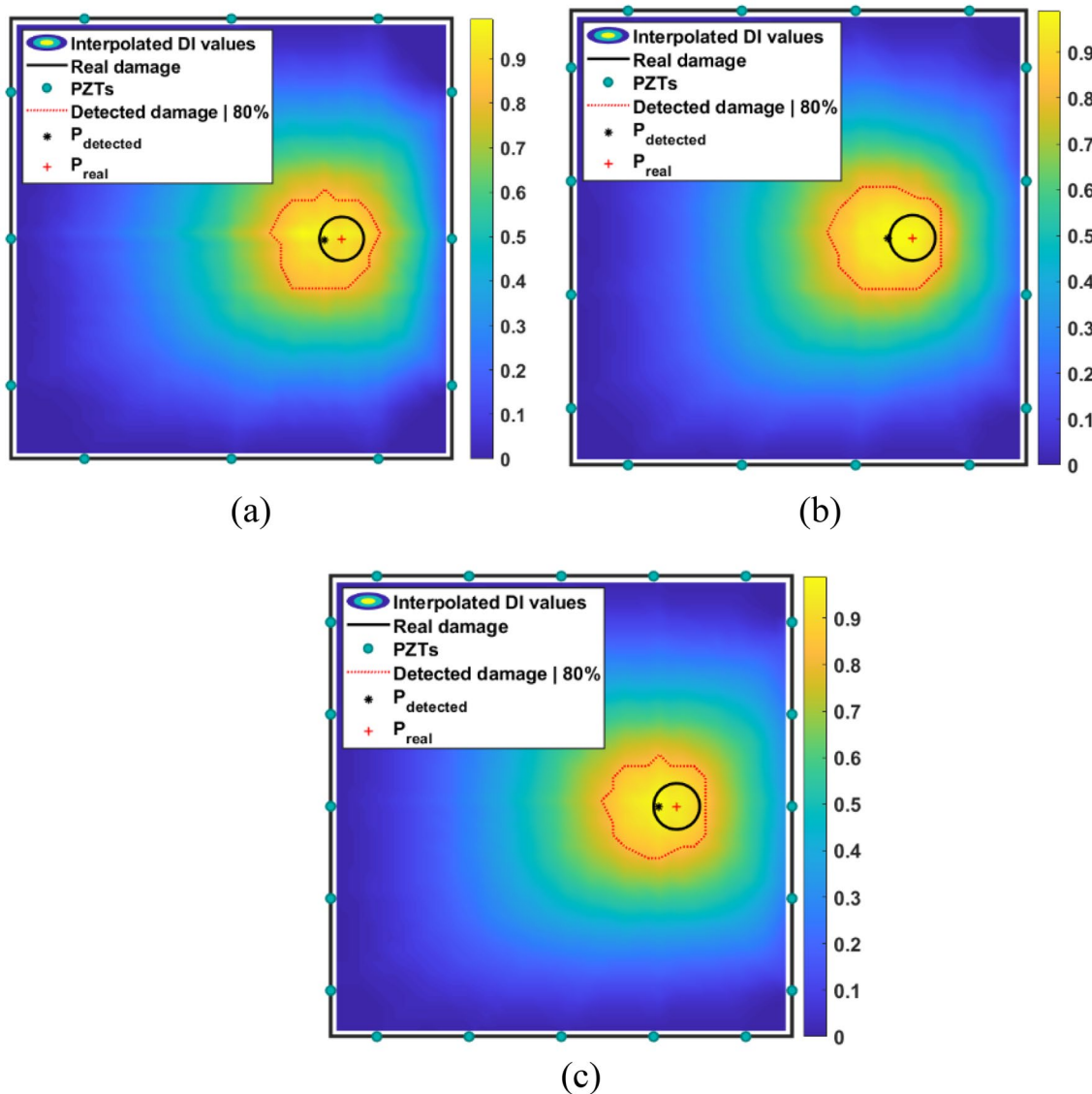


Fig. 14 Damage localization using different number of PZTs and truncation at ToFi; using: **a** 12 PZTs, **b** 16 PZTs, **c** 20 PZTs

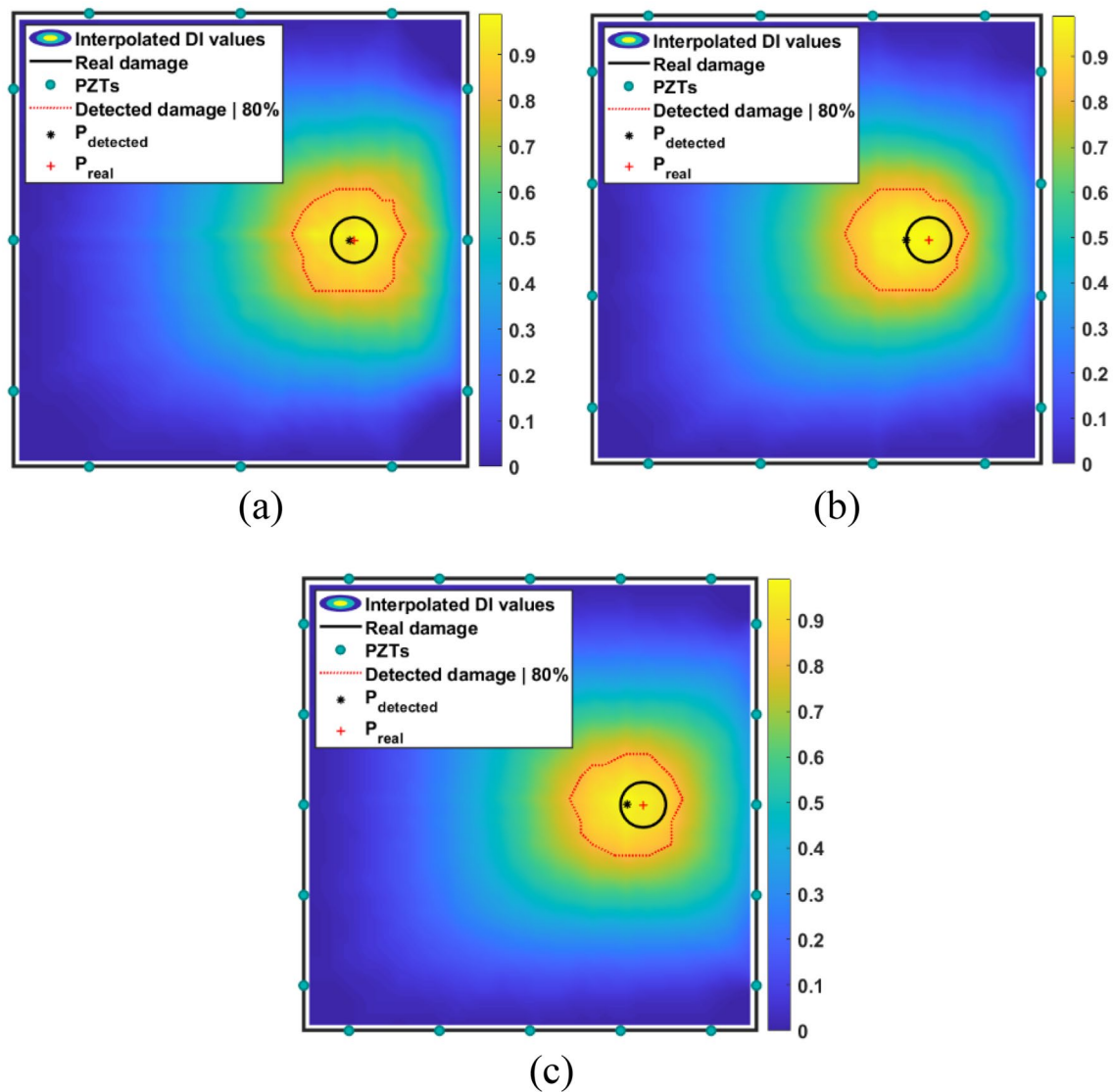


Fig. 15 Damage detection using different number of PZTs and truncation at ToFi; using: **a** 12 PZTs, **b** 16 PZTs, **c** 20 PZTs

As previously described in the methodology section, the ED was calculated for each of the implemented trials. The resulting value of the ED for each trial is summarized in Table 4, which presents the parameter, level of that parameter, and the corresponding ED.

Conclusions and Recommendations

The application of ToF is very important for damage localization with acceptable accuracy. However, according to the authors' best knowledge a clear specification of the proper selection of ToF criteria is missing in the literature. Therefore, this study elaborated part of the missing details of the method. Applying our investigation strategy provides a good and effective method to optimize both numerical and also

experimental investigations on the recent techniques in the field of SHM. Our method achieved a considerable value of the target function after 20 trials, which compares favorably to the factorial number of trials required by other optimization methods to achieve similar results.

Furthermore, applying the investigated hybrid method requires having an intact and damaged state of the specimen and demands the calculation of energy for each acquired signal. Thus, the quality of the information of the signal is very important for the damage detection. In addition, the truncation policy of the recorded signals is mandatory to reach a good damage localization. This gave rise to investigation of the truncation position of each signal to improve damage detection. Based on the results of this investigation the truncation at the ToF of the damaged case of the signal

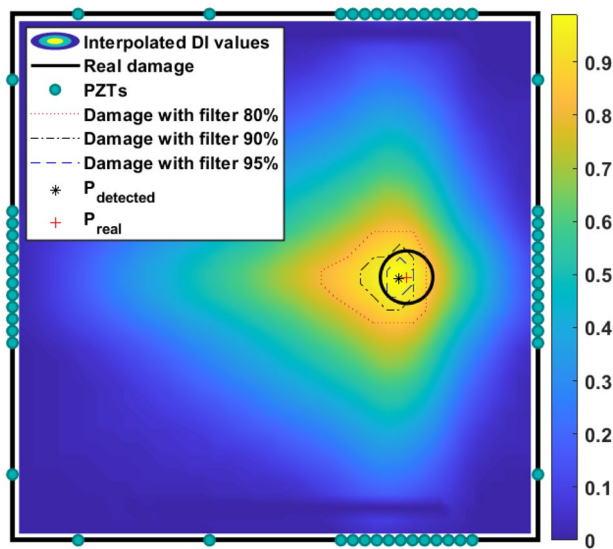


Fig. 16 Damage localization with modified addition of PZTs — addition of 10 PZTs at each side

on each AS-path gives the best damage localization results. However, further investigation is recommended on determining the effective part of the acquired signal to get even better damage localization.

The number of PZTs should be selected sufficiently to suit the mesh-size used in the numerical model of the specimen. In other words, a minimum and a maximum number of elements should be achieved between each two neighbored

PZTs. Furthermore, the number of PZTs used in the damage localization is also depending on the size of the assumed damage to be detected. Therefore, it is recommended to apply further investigations regarding the number of PZTs used for the task of damage localization for other cases such as having more than one-hole, different shapes of damages, different locations of the damages.

To further improve our investigation strategy, future work could include incorporating a decision reward score for selecting parameters in the next group of trials, based on weight factor or reward score. Additionally, applying the strategy to more complex problems would be beneficial.

Regarding the investigated method, further improvement could be achieved by applying our suggested investigation method on other important parameters that affect the performance of the hybrid method such as the material properties and the time increment and the excitation wave used for the damage detection. Additionally, it could be interesting to apply our method on further levels of the investigated parameters of this work. Further, the investigation of the discretization size in the interpolation process of the investigated method represents additional target in the outlook of the research.

Acknowledgements Funded by the German Research Foundation (DFG, Deutsche Forschungsgemeinschaft), Project Nr. 448696650.

Funding Open Access funding enabled and organized by Projekt DEAL.

Table 4 Evaluation results of the investigation strategy

Trial Nr	Parameter	Investigated parameter level	ED
1	ToF	No ToF	0.0615
2	ToF	ToF1	0.0478
3	ToF	ToF2	0.0383
4	ToF	ToF3	0.0367
5	Truncation	No truncation	0.0242
6	Truncation	At ToFi + WD	0.0344
7	Truncation	At ToFd + WD	0.0386
8	Truncation	At ToFi	0.0212
9	Truncation	At ToFd	0.0226
10	Truncation	At ToFi—Boundary Filtered	0.0203
11	Truncation	At ToFd—Boundary Filtered	0.0218
12	Extended Domain	Extended domain	0.0417
13	Extended Domain	Extended domain + signal correction	0.0423
14	number of PZTs	12 PZTs + truncation at ToFi	0.0155
15	number of PZTs	16 PZTs + truncation at ToFi	0.0218
16	number of PZTs	20 PZTs + truncation at ToFi	0.0158
17	number of PZTs	12 PZTs + truncation at ToFd	0.0037
18	number of PZTs	16 PZTs + truncation at ToFd	0.0203
19	number of PZTs	20 PZTs + truncation at ToFd	0.0141
20	number of PZTs	56 PZTs + truncation at ToFd	0.0058

Open Access This article is licensed under a Creative Commons Attribution 4.0 International License, which permits use, sharing, adaptation, distribution and reproduction in any medium or format, as long as you give appropriate credit to the original author(s) and the source, provide a link to the Creative Commons licence, and indicate if changes were made. The images or other third party material in this article are included in the article's Creative Commons licence, unless indicated otherwise in a credit line to the material. If material is not included in the article's Creative Commons licence and your intended use is not permitted by statutory regulation or exceeds the permitted use, you will need to obtain permission directly from the copyright holder. To view a copy of this licence, visit <http://creativecommons.org/licenses/by/4.0/>.

References

- Clough RW, Penzien J (2003) Dynamics of Structures. Computers and Structures Inc, Third Edit
- Diab A, Nestorović T (2021) Convergence Study on Wave Propagation in a Concrete Beam. In: 11th International Workshop NDT in Progress. e-Journal of Nondestructive Testing.
- Diab A, Nestorović T (2023) Damage Index Implementation for Structural Health Monitoring In: Dimitrovová Z, Biswas P, Gonçalves R, Silva T, (eds) Recent Trends in Wave Mechanics and Vibrations. WMVC 2022 Springer, Cham
- Díaz LA, Martín MT, Vampa V (2009) Daubechies wavelet beam and plate finite elements. Finite Elem Anal Des 45:200–209. <https://doi.org/10.1016/J.FINEL.2008.09.006>
- Dr. Erol Kalkan PE (2023) An automated P-phase Arrival Time Picker with SNR output. <https://www.mathworks.com/matlabcentral/fileexchange/57729-an-automated-p-phase-arrival-time-picker-with-snr-output>
- Fan X, Li J, Hao H (2016) Piezoelectric impedance based damage detection in truss bridges based on time frequency ARMA model. Smart Struct Syst. <https://doi.org/10.12989/sss.2016.18.3.501>
- Goyal D, Pabla B (2016) Development of non-contact structural health monitoring system for machine tools. J Appl Res Technol. <https://doi.org/10.1016/j.jart.2016.06.003>
- Goyal D, Pabla BS (2016) The vibration monitoring methods and signal processing techniques for structural health monitoring: a review. Arch Comput Methods Eng 23:585–594. <https://doi.org/10.1007/s11831-015-9145-0>
- Guminiak M, Knitter-Piatkowska A (2018) Selected problems of damage detection in internally supported plates using one-dimensional discrete wavelet transform. J Theor Appl Mech. <https://doi.org/10.15632/jtam-pl.56.3.631>
- Huang JQ (2013) Non-destructive evaluation (NDE) of composites: acoustic emission (AE). Non-Destructive Eval Polym Matrix Compos Tech Appl. <https://doi.org/10.1533/9780857093554.1.12>
- Jahangir H, Hasani H, Esfahani MR (2021) Damage Localization of RC Beams via Wavelet Analysis of Noise Contaminated Modal Curvatures. 5: 101–133. <https://doi.org/10.22115/SCCE.2021.292279.1340>
- Jiang S, Cheng Y, Zhang J (2023) Vision-guided unmanned aerial system for rapid multiple-type damage detection and localization. Struct Heal Monit 22:319–337. <https://doi.org/10.1177/14759217221084878>
- Kalkan E (2016) An automatic p-phase arrival-time picker. Bull Seismol Soc Am 106:971–986. <https://doi.org/10.1785/0120150111>
- Knitter-Piatkowska A, Guminiak M, Przychodzki M (2016) Application of discrete wavelet transformation to defect detection in truss structures with rigidly connected bars. Eng Trans 64:157–170
- Marković N, Nestorović T, Stojić D, Marjanović M, Stojković N (2017) Hybrid approach for two dimensional damage localization using piezoelectric smart aggregates. Mech Res Commun 85:69–75. <https://doi.org/10.1016/j.mechrescom.2017.08.011>
- Ramadas C, Balasubramaniam K, Hood A, Joshi M, Krishnamurthy CV (2011) Modelling of attenuation of Lamb waves using Rayleigh damping: numerical and experimental studies. Compos Struct 93:2020–2025. <https://doi.org/10.1016/J.COMPSTRUCT.2011.02.021>
- Rautela M, Gopalakrishnan S (2021) Ultrasonic guided wave based structural damage detection and localization using model assisted convolutional and recurrent neural networks. Expert Syst Appl. <https://doi.org/10.1016/j.eswa.2020.114189>
- Sattarifar A, Nestorović T, (2021) Feature Generation and Selection for Identification of Damage in Thin-Walled Structures Based on a Statistical Approach In: ASME 2021 Conference on Smart Materials. Adaptive Structures and Intelligent Systems. <https://doi.org/10.1115/SMASIS2021-67538>
- Stojić D, Nestorović T, Marković N, Marjanović M (2018) Experimental and numerical research on damage localization in plate-like concrete structures using hybrid approach. Struct Control Heal Monit. <https://doi.org/10.1002/stc.2214>
- Tian Z, Huo L, Gao W, Li H, Song G (2017) Modeling of the attenuation of stress waves in concrete based on the Rayleigh damping model using time-reversal and PZT transducers. Smart Mater Struct. <https://doi.org/10.1088/1361-665X/aa80c2>
- Vitola J, Pozo F, Tibaduiza DA, Anaya M (2017) Distributed piezoelectric sensor system for damage identification in structures subjected to temperature changes. Sensors. <https://doi.org/10.3390/s17061252>
- Walker JS (2008) A Primer on Wavelets and Their Scientific Applications, 2nd Editio. Chapman and Hall/CRC
- Wang B, Wang X, Hua L, Li J, Xiang Q (2017) Mean grain size detection of DP590 steel plate using a corrected method with electromagnetic acoustic resonance. Ultrasonics 76:208–216. <https://doi.org/10.1016/J.ULTRAS.2016.12.002>
- Wang P, Shi Q (2018) Damage identification in structures based on energy curvature difference of wavelet packet transform. Shock Vib 2018:4830391. <https://doi.org/10.1155/2018/4830391>
- Wu Q, Okabe Y, Yu F (2018) Ultrasonic structural health monitoring using fiber Bragg grating. Sensors 18:3395. <https://doi.org/10.3390/s18103395>
- Yang H, Xu X, Neumann I (2016) Laser scanning-based updating of a finite-element model for structural health monitoring. IEEE Sens J 16:2100–2104. <https://doi.org/10.1109/JSEN.2015.2508965>
- Yang Y, Hu Y, Lu Y (2008) Sensitivity of PZT impedance sensors for damage detection of concrete structures. Sensors 8:327–346. <https://doi.org/10.3390/s8010327>
- Yue N, Khodaei ZS, Aliabadi MH (2021) Damage detection in large composite stiffened panels based on a novel SHM building block philosophy. Smart Mater Struct 30:45004. <https://doi.org/10.1088/1361-665X/abe4b4>

Publisher's Note Springer Nature remains neutral with regard to jurisdictional claims in published maps and institutional affiliations.

